Primary amines as ligands and linkers in complexes of tripyrrindione radicals

Iva Habenšus, Ameen Ghavam, Clayton J. Curtis, Andrei V. Astashkin, Elisa Tomat*

Department of Chemistry and Biochemistry, The University of Arizona, 1306 E. University Blvd., Tucson, AZ 85721-0041, USA

Dedicated to Prof. Jonathan L. Sessler on the occasion of his 65th birthday

ABSTRACT: Biopyrrin pigments, which result from the degradation of heme in biological settings, feature three or two pyrrole rings and characteristic pyrrolin-2-one termini. These scaffolds serve as redox-active ligands and electron reservoirs in coordination compounds. Tripyrrin-1,14-dione coordinates divalent transition metals as a dianionic ligand hosting a delocalized radical. Herein, we report the synthesis and characterization of palladium(II) and platinum(II) tripyrrindione complexes featuring a primary amine (i.e., aniline, tert-butylamine, 1,2-ethylenediamine) at the fourth coordination site within square planar geometries. Interligand hydrogen-bonding interactions are observed between the coordinated amine and the carbonyl groups on the tripyrrindione scaffold. Notably, 1,2-ethylenediamine is employed to link two Pt(II) tripyrrindione complexes. As revealed by optical absorption and electron paramagnetic resonance (EPR) spectroscopy, all resulting complexes present ligand-based radicals that are stable at room temperature and when exposed to air. Spin pairing through multicenter interactions leads to π-dimerization of the tripyrrindione radicals and decrease of the EPR signal at low temperature. Electrochemical measurements confirm that the ligand system undergoes quasi-reversible one-electron oxidation and reduction, thus confirming the ability of tripyrrindione to form square planar complexes in three different redox states.

KEYWORDS: tripyrrindione, hydrogen bonding, primary amine, linker, palladium, platinum.

*Correspondence to: Elisa Tomat, tel.: +1 520 626 5714, email: tomat@arizona.edu

INTRODUCTION

Linear oligopyrroles are common pigments found in biology as precursors or metabolites of tetrapyrrolic macrocycles as well as chromophores in photosynthetic systems [1,2]. Synthetic analogs with oligopyrrolic chains of various lengths have a rich coordination chemistry [3–6], which has led to the development of several sensors [7]. Among the biologically occurring scaffolds, biliverdin (Chart 1) and its synthetic bilindione analogs were found to stabilize ligand-based radicals in multiple transition metal complexes [8]. This ability to serve as redox-active ligands is also shared by smaller biopyrrins, which feature three or two pyrrole rings and the characteristic pyrrolin-2-one termini [9]. Just as the macrocyclic tetrapyrroles, such as porphyrins and corroles, multiple complexes of bilindiones and smaller biopyrrins present frontier molecular orbitals of predominantly ligand character and therefore host redox equivalents on the conjugated ligand π systems. As such, redox-active oligopyrrolic ligands are of interest not only for the development of redox-responsive sensors but also for the design of redox catalysts and functional materials.

Chart 1. Examples of naturally occurring and synthetic bilin pigments and bipyrrin ligands and their metal complexes

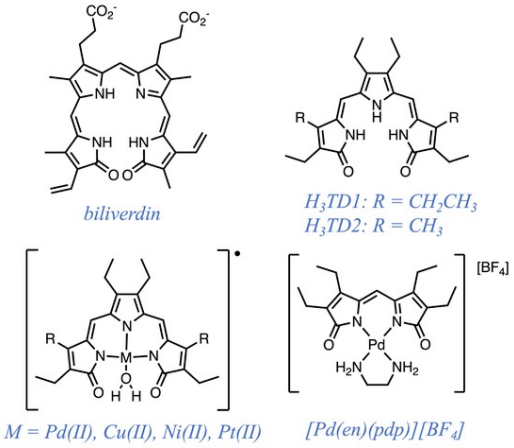

The tripyrrin-1,14-dione ligand (H_3TD1 and H_3TD2, Chart 1), which features the scaffold of the urinary pigment uroerythrin [10,11], coordinates palladium(II) [12], copper(II) [13,14], nickel(II) [13], and platinum(II) [15] as a tridentate dianionic radical (i.e., formally $TD1^{2-\bullet}$ or $TD2^{2-\bullet}$). Within several square planar complexes reported so far (Chart 1), an aqua ligand occupies the fourth coordination site and is stabilized by two hydrogen-bonding interactions to the carbonyl groups of the tripyrrindione ligand. The calculated strength of each interaction is ~9.5 kcal·mol^{-1} [12], consistent with the tendency of these compounds to bind adventitious water even in the presence of other coordinating species such as the acetate anion. Hydrogen-bound, bridging aqua ligands were also observed in the binuclear structure of zinc(II) tripyrrindione, which was characterized as a fluorescent radical in solution [16].

Hydrogen-bonding interactions are an important component of the chemistry of linear oligopyrroles both in free ligands [17–20] and in metal complexes. Several palladium(II) dipyrrin-1,9-dione complexes feature intraligand hydrogen bonds involving the carbonyl group and aqua ligands [21], bridging hydroxido ligands [21], as well as aliphatic and aromatic primary amines (e.g., [Pd(en)(pdp)][BF_4], Chart 1) [22]. These observations prompted us to investigate the coordination of primary amines in tripyrrindione complexes and examine their effect on the properties of these complexes. In particular, we reasoned that diamine ligands could be employed to connect tripyrrindione complexes and therefore provide access to diradical systems.

Because we observed that the displacement of the aqua ligand is not easily achievable at room temperature, we sought to develop synthetic methods for the coordination of the amine ligands. We report the synthesis of palladium(II) and platinum(II) tripyrrindione complexes with primary amine ligands (both aromatic and aliphatic), thus demonstrating the ability to coordinate a ligand other than water in the fourth coordination site while preserving the hydrogen-bonding interactions that stabilize the primary coordination sphere.

RESULTS AND DISCUSSION

Synthesis of metal complexes

Most previously reported tripyrrindione complexes feature ethyl substituents on the β positions of all three pyrrolic units (H_3TD1, Chart 1) [17]. For this study, we worked with the recently reported analog H_3TD2 (Chart 1), which is prepared from the condensation of 3,4-diethyl-2,5-diformylpyrrole with commercially available 3-ethyl-4-methyl-3-pyrrolin-2-one [15]. For the metal coordination reactions in the presence of primary amine ligands, we sought to work in anhydrous conditions to avoid the coordination of adventitious water: all glassware was flame-dried, all solvents were thoroughly dried over molecular sieves, and the primary amines were distilled prior to use. The metal insertions occur upon one-electron oxidation of the ligand in the presence of oxygen: to maintain anhydrous conditions, the reaction mixtures were exposed to air through a drying tube or slowly bubbled with dry oxygen from a gas cylinder.

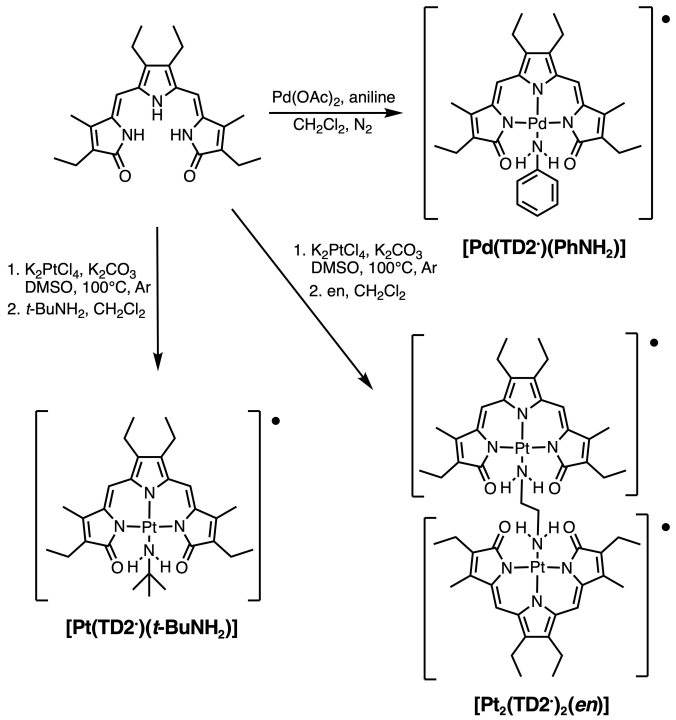

Scheme 1. Synthesis of square planar Pd(II) and Pt(II) complexes containing the tripyrrindione ($TD2^{2-\bullet}$) ligand and neutral primary amines (en= 1,2-ethylenediamine).

As previously reported for the synthesis of [Pd($TD1^{\bullet}$)(H_2O)] [12], the tripyrrindione ligand coordinated Pd(II) at room temperature in the presence of the acetate salt. The aniline complex was synthesized by cannulating a solution of $Pd(OAc)_2$ in dry CH_2Cl_2 into a solution of H_3TD2 and aniline in dry CH_2Cl_2. The reaction mixture was stirred for 24 h, and the desired

product was then isolated by crystallization as a dark blue solid (Scheme 1). The optical absorption spectrum of the product was very similar to that of the previously reported aqua complex, therefore further characterization was necessary to confirm the formation of the desired aniline complex (*vide infra*).

With the goal of synthesizing stable tripyrrindione complexes with primary amine ligands, we also pursued the coordination of platinum(II), which is rather inert to ligand substitution and forms stable amine complexes, including cisplatin and other platinum-based anticancer drugs [23]. As in the case of [Pt(TD2$^{\bullet}$)(H_2O)] [15], the reaction did not proceed at room temperature and required a different preparation relative to the Pd(II) analog. The free ligand H_3TD2, K_2CO_3, and K_2PtCl_4 were dissolved in dry DMSO under argon and the solution was heated at 100 °C for 1 h. The reaction progress was monitored *via* optical absorption spectroscopy: a color change of the reaction mixture from a red to royal blue was observed, likely indicating the formation of a Pt(II) complex that could not be isolated for full characterization. After the ligand was consumed (as indicated by the optical absorption data), the reaction mixture was allowed to cool to room temperature, and the amine ligand (i.e., *t*-$BuNH_2$ or ethylenediamine) was added as a concentrated solution in dry CH_2Cl_2. The solution was exposed to dry air or oxygen and stirred for 3 h. Following an aqueous work-up, the desired Pt(II) complexes were purified by column chromatography and isolated by crystallization from CH_2Cl_2 and pentane. High-resolution mass spectrometry and elemental analysis confirmed the coordination of the primary amines and the formation of complexes [Pd(TD2$^{\bullet}$)($PhNH_2$)], [Pt(TD2$^{\bullet}$)(*t*-$BuNH_2$)], and [Pt_2(TD2$^{\bullet}$)$_2$(en)] (Scheme 1).

Spectroscopic characterization in solution

In all cases, the starting ligand H_3TD2 featuring an absorption band at 487 nm was converted into complexes presenting a main band at 590-600 nm and several weaker bands in the red and near-infrared region, including a distinct band between 939-970 nm (Fig. 1). These long-wavelength bands were previously assigned as intraligand π–π charge transfer bands and are characteristic of metal-bound tripyrrindione radicals. Overall, the observed absorption changes are similar to those we observed upon formation of complexes featuring a tridentate tripyrrindione radical and an aqua ligand in the fourth coordination site [12–16].

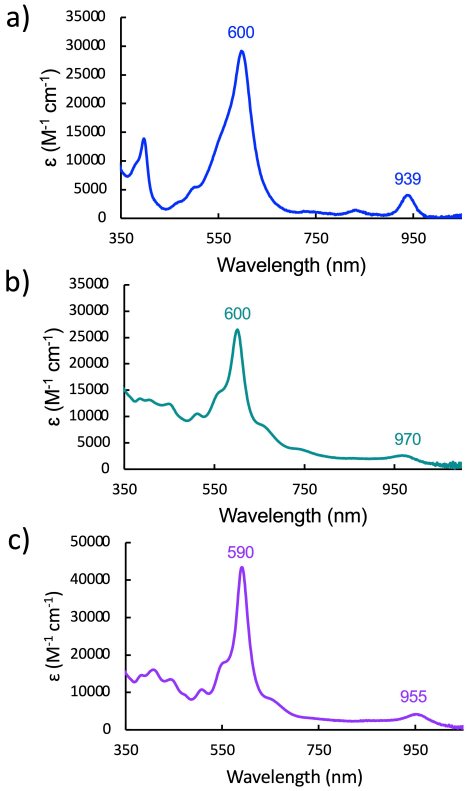

Fig. 1. UV-vis absorption spectra in CH_2Cl_2 of a) [Pd(TD2•)($PhNH_2$)], b) [Pt(TD2•)(*t*-$BuNH_2$)], and c) [Pt_2(TD2•)$_2$(en)].

While working on the synthesis of these amine complexes, the unwanted formation of a minor fraction of aqua complexes was noted in the presence of adventitious water when the solvents or reagents were not properly dried. In the case of the Pt(II) complexes, this impurity could be removed by column chromatography. Notably, once the amine ligand was coordinated, no displacement by water was observed. In addition to the coordination to rather kinetically inert Pd(II) and Pt(II), the hydrogen-bonding interactions within the primary coordination sphere of these complexes (*vide infra*) likely contributed to the stabilization of the primary amine ligands with respect to ligand exchange during purification and isolation.

The observed optical absorption profiles of all three complexes (Fig. 1) are consistent with the tripyrrindione binding as a tridentate dianionic ligand and hosting an unpaired electron delocalized across the scaffold. Indeed, all the isolated compounds were found to be paramagnetic and were investigated by electron paramagnetic resonance (EPR) spectroscopy.

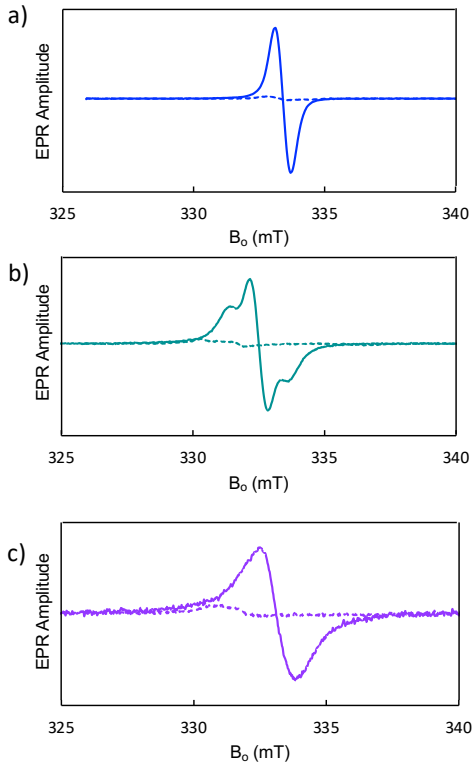

Fig 2. EPR spectra at room temperature (300 K, solid lines) and 160 K (dashed lines) of a) 1 mM [Pd(TD2•)($PhNH_2$)], b) 1 mM [Pt(TD2•)(*t*-$BuNH_2$)], and c) 0.5 mM [Pt_2(TD2•)$_2$(en)] in toluene. Experimental conditions: mw frequency, 9.349 GHz; mw power, 20 μW; field modulation amplitude, 0.1 mT.

The EPR spectrum for [Pd(TD2•)($PhNH_2$)] at room temperature (Fig. 2a) was similar to that observed previously for [Pd(TD1•)(H_2O)]: a single isotropic line with a width of 0.62 mT, located at $g = 2.004$. In contrast, the spectrum of [Pt(TD2•)(*t*-$BuNH_2$)] (Fig. 2b) exhibits a partially resolved triplet centered at $g = 2.008$, with the outer lines due to the isotropic hyperfine interaction (hfi) with the ^{195}Pt nucleus ($I = ½$, natural abundance 33.8%). For the [Pt_2(TD2•)$_2$(en)] sample, the EPR spectrum (Fig. 2c) exhibits a single line with a width of 1.38 mT, located at $g = 2.005$. In this case, the hyperfine splitting from the ^{195}Pt isotope is not resolved because of line broadening caused by slow dynamic spin exchange, an effect that was described and analyzed for similar complexes [15].

In general, the EPR spectra of all three amine complexes are consistent with an unpaired electron delocalized over the tripyrrindione ligand, with only a minor portion of the spin density (less than 10%) located on the metal centers. We have previously observed that the Pd(II) and Cu(II) tripyrrindione aqua complexes form EPR-silent π-dimers at low temperatures through antiferromagnetic coupling of the ligand-based spins [14]. These π-stacked dimers result from multicentered interactions between delocalized organic radicals that are often described as "pancake bonds" [24,25].

To investigate the formation of π-dimers in the case of these amine complexes, we conducted variable-temperature EPR measurements. The EPR spectra of [Pd(TD2•)($PhNH_2$)] (1 mM), [Pt(TD2•)(*t*-$BuNH_2$)] (1 mM), and [Pt_2(TD2•)$_2$(en)] (0.5 mM) in toluene were recorded at nonsaturating microwave (mw) power levels between 340 K and 160 K. The double integrals of these spectra over the magnetic field were multiplied by the absolute temperature to obtain the relative spin concentrations as a function of temperature (Fig. 3). For the [Pd(TD2•)($PhNH_2$)] and [Pt(TD2•)(*t*-$BuNH_2$)] complexes, the temperature dependance of the spin concentration was modeled as resulting from a simple equilibrium between monomeric tripyrrindione

radicals and EPR-silent π-dimer. A direct least-squares fitting of the EPR temperature dependences (see Supporting Information) afforded the thermodynamic parameters of the dimerization reaction (Table 1). The Δ*H* and Δ*S* values are similar to those of Pd(II), Cu(II), and Pt(II) tripyrrindiones with aqua ligands in the fourth coordination site [14,15]. As such, the thermodanymic drive to dimerization for Pd(TD2•)($PhNH_2$)] and [Pt(TD2•)(*t*-$BuNH_2$)] is not hindered by the aliphatic or aromatic groups on the amine ligands.

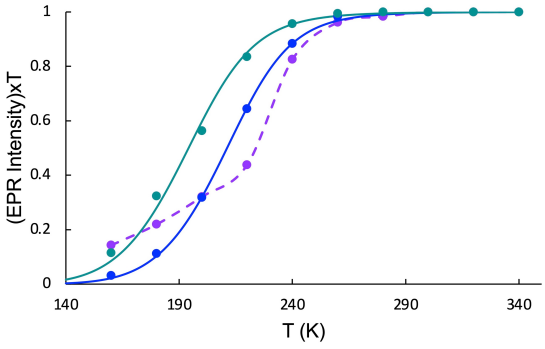

Fig 3. Temperature dependences of relative spin concentrations for 1 mM [Pt(TD2•)(*t*-$BuNH_2$)] (green), 1 mM [Pd(TD2•)($PhNH_2$)] (blue), and 0.5 mM [Pt_2(TD2•)$_2$(en)] (purple) in toluene. The 0.5 mM concentration of [Pt_2(TD2•)$_2$(en)] corresponds to 1 mM radical units, as in the other two complexes. The experimental points are shown as dots. The green and blue solid lines are the simulations obtained by direct least-squares fitting. The resulting thermodynamic parameters are in Table 1. The purple dashed line is a spline interpolation shown for visual guidance only.

Table 1. Thermodynamic parameters of dimerization of [Pd(TD2•)($PhNH_2$)], [Pt(TD2•)(*t*-$BuNH_2$)], and previously reported complexes in toluene

Complex	Δ*H* (kcal mol^{-1})	ΔS (cal mol^{-1} K^{-1})
Pd(TD1•)(H_2O)	-9.9 ± 0.3	-29 ± 1.5
Cu(TD1•)(H_2O)	-8.6 ± 0.3	-30 ± 1.5
Pt(TD2•)(H_2O)	-8.8 ± 0.4	-23 ± 1
[Pd(TD2•)($PhNH_2$)]	-9.1 ± 0.4	-29 ± 1
[Pt(TD2•)(*t*-$BuNH_2$)]	-7.5 ± 0.4	-25 ± 1

For the [Pt_2(TD2•)$_2$(en)] complex, the interpretation of the EPR temperature dependence is more complicated. This complex contains two PtTD2 radical units, each available to form a dimer with another radical in a different complex. As a result, these complexes can form linear oligomers of various lengths, and each such oligomer will have two paramagnetic PtTD2 units at its ends. An *intramolecular* π-dimerization of the two Pt(II) tripyrrindione units in parallel (i.e., head-to-head) orientation could also be considered; however, this type of dimers is not observed in our structural analysis (*vide infra*) and in other trypyrrindione radicals [14,15]. Overall, the temperature dependance of the EPR signal for [Pt_2(TD2•)$_2$(en)] (Fig. 3) is attributable to multiple dimerization equilibria. Therefore, the associated thermodynamic parameters could not be derived.

Structural characterization in the solid state

Single crystals suitable for X-ray diffraction analysis (Table S1) were obtained by slow evaporation of solutions of [Pd(TD2•)($PhNH_2$)] and [Pt(TD2•)(*t*-$BuNH_2$)] in a CH_2Cl_2/pentane mixture and by slow diffusion of pentane into a solution of [Pt_2(TD2•)$_2$(en)] in CH_2Cl_2. The crystal structures (Figs. 4-5, S1-S3) reveal Pd(II) or Pt(II) complexes with coordinated primary amines that are hydrogen-bound to both carbonyl groups of the tridentate tripyrrindione ligand. All aminic hydrogen atoms engaged in hydrogen bonding were located in the Fourier maps during structure refinement. In [Pt_2(TD2•)$_2$(en)], two Pt(II) tripyrrindione complexes are tethered by the ethylene diamine ligand.

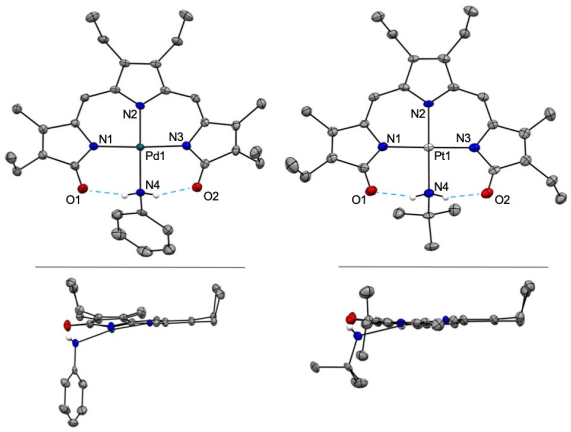

Fig. 4. Crystal structures of [Pd(TD2•)($PhNH_2$)] (left) and [Pt(TD2•)(*t*-$BuNH_2$)] (right) showing a partial labeling scheme. Carbon-bound hydrogens are omitted for clarity. Non-hydrogen atoms are displayed as thermal displacement ellipsoids set at the 50% probability level. CCDC: 2231917 (left), 2231918 (right).

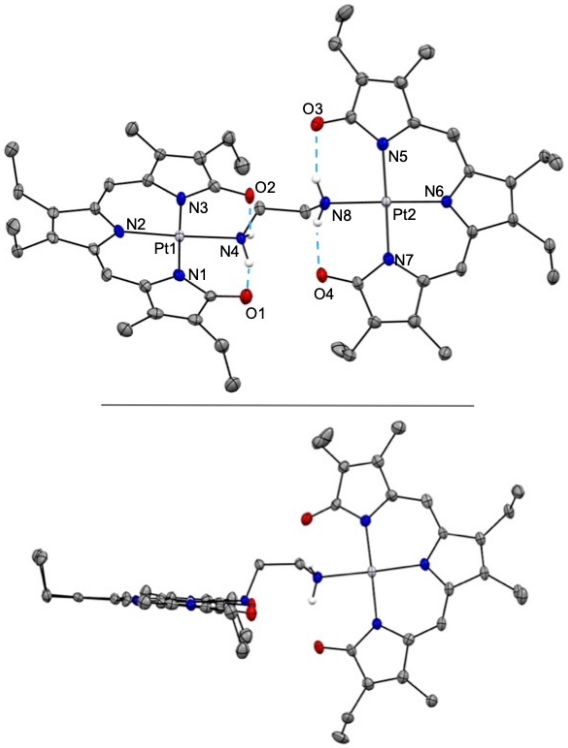

Fig. 5. Crystal structure of [$Pt_2(TD2^{\bullet})_2$(en)] showing a partial labeling scheme. Carbon-bound hydrogens as well as two solvent molecules (CH_2Cl_2) are omitted for clarity. Non-hydrogen atoms are displayed as thermal displacement ellipsoids set at the 50% probability level. CCDC: 2231916.

Table 2. Comparison of hydrogen-bonding donor-acceptor distances and carbonyl stretching frequencies of the amine complexes in the solid state

	$N_{amine}\cdots O_{TD2}$ (Å)	ν_{CO} (cm^{-1})
H_3TD2	-	1677
[$Pd(TD2^{\bullet})(PhNH_2)$]	2.679 2.697	1637
[$Pt(TD2^{\bullet})$(*t*-$BuNH_2$)]	2.684 2.725	1646
[$Pt_2(TD2^{\bullet})_2$(en)]	2.657 2.663 2.671 2.676	1641

The metal centers lie in the plane of the tripyrrindione nitrogen donors, whereas the aniline and the *tert*- butyl amine nitrogen donors are respectively 10.3º and 6.9º out of plane, leading to a geometry that is generally comparable to that of [$Pd(TD1^{\bullet})(H_2O)$]. In contrast, the *tert*-butyl amine *N*-donor in a Pd(II) tripyrrin was observed 24º out of plane, likely owing to the 1,14-dimethyl substitution of the tripyrrin ligand, which presented steric hinderance rather than hydrogen-bonding interactions [26]. The bond lengths on the tripyrrindione framework (Table S2) are similar to those observed in previously reported complexes of this ligand [12,13,16], thus confirming the redox state of a conjugated $TD2^{2-\bullet}$ ligand with two carbonyl groups at the terminal pyrrolic units.

The donor-acceptor distances for the hydrogen bonds between the amine nitrogen atoms and the carbonyl oxygens (Table 2) are indicative of robust interactions. This observation is also reflected in the IR spectroscopy data, which were collected in the solid state and assigned according to prior analyses of bilirubin (see Experimental Section) [27,28]. In particular, the lactam C=O stretching frequencies for the amine metal complexes (i.e., 1637-1646 cm^{-1}, Table 2) are consistently red-shifted relative to the band at 1677 cm^{-1} for the free ligand H_3TD2.

The crystal structures of [$Pt(TD2^{\bullet})$(*t*-$BuNH_2$)] and [$Pt_2(TD2^{\bullet})_2$(en)] show comparable π stacking geometries (Figs. S5-S6), with antiparallel orientation of the complexes. The interplanar distances for the stacked pairs of these complexes (3.287 Å and 3.377 Å, respectively) are similar to those previously observed for [$Pd(TD1^{\bullet})(H_2O)$] and [$Pt(TD2^{\bullet})(H_2O)$] (~3.3 Å). The Pt-Pt distances are, respectively, 4.574 Å and 4.977 Å. In contrast, within the packing structure of [$Pd(TD2^{\bullet})(PhNH_2)$] (Fig. S4), the relative orientation of the ethyl substituents and the aniline phenyl group appears to prevent effective π overlap and stacking. The complexes are arranged in antiparallel orientation, but are shifted laterally by about 7 Å. As a result, the metal-metal distance in the pair (~8.03 Å) is significantly longer than those found in the other complexes in this series. In solution, however, the ethyl groups can adopt a variety of orientations, thus allowing for the multicenter interaction between tripyrrindione radicals. Indeed, the temperature dependence of the EPR signal (blue trace in Fig. 3) and the thermodynamic parameters of dimerization for [$Pd(TD2^{\bullet})(PhNH_2)$] (Table 1) are similar to those of the other studied complexes and indicate that the π stacking and dimerization occur in solution.

Electrochemical characterization

The electrochemical profiles of [Pd(TD2•)($PhNH_2$)], [Pt(TD2•)(*t*-$BuNH_2$)], and [Pt_2(TD2•)$_2$(en)] were investigated by cyclic voltammetry in CH_2Cl_2, and the observed potentials were referenced to the ferrocene/ferrocenium couple (Fc/Fc^+) (Fig. 6). In spite of the different metal centers and amine ligands, the voltammograms of [Pd(TD2•)($PhNH_2$)] and [Pt(TD2•)(*t*-$BuNH_2$)] are quite similar and display two quasi-reversible events assigned to tripyrrindione-based one-electron oxidations (at -0.294 V and -0.258 V, respectively) and reductions (at -0.904 V and -0.845 V). When compared to the aqua complexes [Pd(TD1•)(H_2O)] and [Pt(TD2•)(H_2O)] (with oxidations at -0.052 V and -0.107, and reductions at -0.672 V and -0.701 V, respectively), both events for the amine complexes are shifted cathodically by ~200 mV. As such, the replacement of the aqua ligand with a primary amine, namely a better σ donor, has an effect on the electrochemical profile of the bound tripyrrindione, which becomes harder to reduce and easier to oxidize.

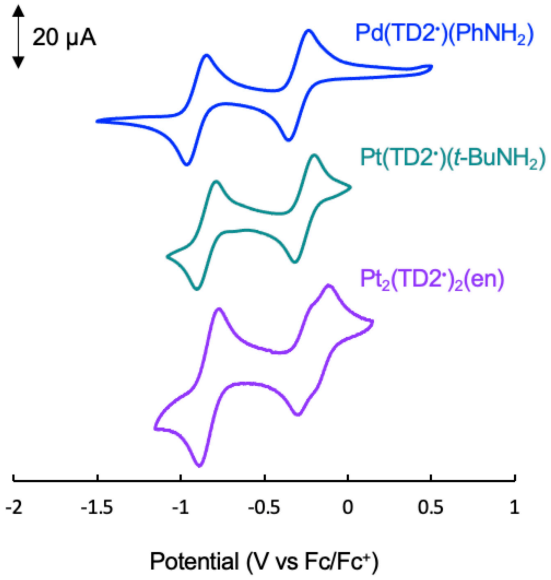

Fig. 6. Cyclic voltammograms of [Pd(TD2•)($PhNH_2$)], [Pt(TD2•)(*t*-$BuNH_2$)], and [Pt_2(TD2•)$_2$(en)] (1-2 mM) at a glassy carbon electrode in CH_2Cl_2 with 0.1 M [(*n*-Bu_4)(PF_6)] as a supporting electrolyte. Data collected at a 100 $mV{\cdot}s^{-1}$ scan rate using a $Ag/AgNO_3$ reference electrode and a Pt wire auxiliary electrode.

Similar half-wave potentials are observed for the voltammogram of [Pt_2(TD2•)$_2$(en)] (Fig. 6), which shows one quasi-reversible reduction at -0.832 mV and two quasi-reversible oxidation events at -0.259 and -0.157 mV. The current associated with the reductive event is larger (about 1.7 times) than those for the two oxidations and is assigned to two ligand-based reductions of the linked Pt(II) tripyrrindione units occurring independently at the same potential. The relatively small difference between the half-wave potentials of the oxidation events (102 mV) suggests slight delocalization of the first oxidizing equivalent over the two ligands. The overall complex is thus categorized to class II in the Robin-Day classification of mixed-valence compounds [29]; however, electrostatic and solvation energy effects could also account for the small difference in redox potential for the neutral/monocationic vs monocationic/dicationic pairs in this species featuring two linked complexes.

EXPERIMENTAL

General Methods

H_3TD2 was synthesized according to a previously reported procedure [15]. Dichloromethane (CH_2Cl_2), pentane and THF were dried by passage through a solvent purifier. DMSO was dried over activated molecular sieves (4 Å). Dry solvents were confirmed to contain <0.1 ppm H_2O using a Mettler Toledo C10S Coulometric Karl Fisher Titrator. Amine reagents were freshly distilled prior to use. All other commercial reagents were used without further purification. UV-visible spectra were obtained at ambient temperature using an Agilent 8453 UV–vis spectrophotometer or an Agilent Cary 60 UV–vis spectrophotometer. Infrared (IR) measurements were performed on a Thermo Nicolet iS5 with an iD7 ATR accessory containing a diamond plate and measured using the Thermo Ominic 9 program. A background was collected and then a solid sample was placed directly on the diamond plate to be analyzed. High-resolution mass spectrometry data were acquired at the University of Arizona Mass Spectrometry Core Facility. Elemental analyses were performed by Numega Resonance Labs, San Diego, CA. NMR spectra were recorded on a Bruker NEO-500 MHz NMR spectrometer at the NMR Spectroscopy Facility of the Department of Chemistry and Biochemistry at The University of Arizona. The continuous-wave (CW) EPR experiments were carried out at EPR facility of the Department of Chemistry and Biochemistry (UArizona) on an X-band EPR spectrometer Elexsys E500 (Bruker Biospin) equipped with a rectangular TE_{102} resonator. The variable temperature measurements were performed using the cryogenic nitrogen gas flow system ER 4111VT (Bruker).

Synthetic procedures

[Pd(TD2•)(PhNH₂)]. H_3TD2 (26 mg, 0.066 mmol) was placed in a Schlenk flask and dissolved in dry CH_2Cl_2 (2 mL) over activated molecular sieves (3 Å) and in the presence of dry O_2. Freshly distilled aniline (20 μL, 0.230 mmol) was added using a syringe and then a solution of palladium acetate (31 mg, 0.138 mmol) in dry CH_2Cl_2 (2 mL) was added via cannula transfer. The reaction mixture was stirred overnight at room temperature, gradually changing color from red to a deep blue. The solvent was mostly evaporated from the Schlenk flask, and dry pentane (20 mL) was added via cannula. The solution was swirled and a long needle inserted to just above solvent line to facilitate evaporation. Crystals grew along the walls of the flask as the solvent evaporated (21 mg, 54%). UV–Vis (CH_2Cl_2) λ_{max} (ε) 397 (13,900), 600 (28,700), 731 (1400), 832 (1,500), 939 nm (3,900 $M^{-1}cm^{-1}$). ν (cm^{-1}): 2963 (CH), 2929 (CH), 2871 (CH), 1677 (C=O), 1626 (C=C), 1603 (C=C). HRMS-ESI$^+$ (*m/z*): $[M]^+$ calcd for $[C_{30}H_{35}N_4O_2Pd]$, 589.18008; found 589.17877. Anal. Calcd. for $[C_{30}H_{35}N_4O_2Pd]\bullet(H_2O)$: C, 59.3; H, 6.1; N, 9.2%; found: C, 59.3; H, 5.6; N, 9.4%.

[Pt(TD2•)(t-BuNH₂)]. H_3TD2 (20 mg, 0.051 mmol), K_2PtCl_4 (22.2 mg, 0.053 mmol), and K_2CO_3 (21.1 mg, 0.152 mmol) were dissolved in dry DMSO (0.5 mL) and heated at 100 °C for 1 h under an argon atmosphere. Upon consumption of free H_3TD2, as determined through UV–visible absorption spectroscopy, the reaction was cooled to room temperature. *t*-$BuNH_2$ (53.4 µL, 0.508 mmol) was dissolved in dry CH_2Cl_2 (3 mL) and added to the reaction mixture, which was stirred at room temperature under argon for an additional 5 min. The navy blue solution was then briefly bubbled with dry oxygen (3-5 min) and then stirred for an additional 3 h to allow for complete oxidation to the radical product. The reaction mixture was diluted with CH_2Cl_2 (50 mL), washed in a separatory funnel with brine (3 x 50 mL) and dried over Na_2SO_4, then the solvent was removed *in vacuo*. The crude solid was purified *via* flash chromatography (0/100 to 35/65, v/v, hexanes/ethyl acetate) to afford [Pt(TD2•)(*t*-$BuNH_2$)] as a teal blue solid. Crystals suitable for X-ray diffraction were grown from slow evaporation of

CH_2Cl_2/pentane (20 mg, 59 %) . UV−Vis (CH_2Cl_2) λ_{max} (ε) 305 (28,400), 385 (11,000), 405 (10,800), 447 (9,300), 511 (7,400), 560 (11,300), 600 (26,400), 655 (7,300), 740 (2,800), 970 nm (2,600 $M^{-1}cm^{-1}$). *v* (cm^{-1}): 3062 w (NH), 2965 (CH), 2929 (CH), 2869 (CH), 1637 (C=O), 1601 (C=C), 1590 (C=C). HRMS-ESI$^+$ (*m/z*): $[M]^+$ calcd for $[C_{28}H_{39}N_4O_2Pt]$, 658.27177; found 658.27173. Anal. Calcd. for $[C_{28}H_{39}N_4O_2Pt]$: C, 51.1; H, 6.0; N, 8.5%; found: C, 51.4; H, 5.3; N, 8.1%.

[Pt$_2$(TD2$^{\bullet}$)$_2$(en)]. H_3TD2 (20.6 mg, 0.052 mmol), K_2PtCl_4 (22 mg, 0.053 mmol), and K_2CO_3 (21.8 mg, 0.158 mmol) were dissolved in dry DMSO (0.5 mL) and heated at 100 °C for 1 h under an argon atmosphere. Upon consumption of free H_3TD2, as determined through UV–visible absorption spectroscopy, the reaction was cooled to room temperature. Ethylenediamine (1.8 μL, 0.027mmol) was dissolved in dry CH_2Cl_2 (3 mL) and added to the reaction mixture dropwise over 5 min and the mixture was stirred at room temperature under argon for an additional 5 min. The navy blue solution was then briefly bubbled with dry oxygen (3-5 min) and then stirred for an additional 3 h to allow for complete oxidation to the radical product. The reaction mixture was diluted with CH_2Cl_2 (50 mL), washed in a separatory funnel with brine (3 x 50 mL) and dried over Na_2SO_4, then the solvent was removed *in vacuo*. The crude solid was purified *via* flash chromatography (0/100 to 50/50, v/v, hexanes/ethyl acetate) to afford [Pt$_2$(TD2$^{\bullet}$)$_2$(en)] as a sapphire blue solid (17 mg, 52%). Crystals suitable for X-ray diffraction were grown from slow evaporation of CH_2Cl_2/pentane . UV−Vis (CH_2Cl_2) λ_{max} (ε) 305 (43,300), 381 (15,400), 407 (17,000), 442 (14,300), 508 (11,400), 550 (18,700), 590 (45,100), 645 (8.900), 955 nm (4,300 $M^{-1}cm^{-1}$). *v* (cm^{-1}): 3200-3050 br (NH), 2961 (CH), 2928 (CH), 2869 (CH), 1641 (C=O), 1610 (C=C). HRMS-ESI$^+$ (*m/z*): $[M+H]^{+2}$ calcd for $[C_{50}H_{64}N_8O_4Pt_2]$, 615.21961; found 615.21625. Anal. Calcd. for $[C_{50}H_{64}N_8O_4Pt_2]\bullet 2(CH_2Cl_2)$: C, 44.6; H, 4.9; N, 8.0%; found: C, 44.8; H, 4.9; N, 8.1%.

X-ray diffraction analysis

The single crystal X-ray diffraction (XRD) experiments were performed at the XRD Facility of the Department of Chemistry and Biochemistry of the University of Arizona. The measurements for [Pd(TD2$^{\bullet}$)($PhNH_2$)] and [Pt$_2$(TD2$^{\bullet}$)$_2$(en)] were conducted on a Bruker Kappa APEX II DUO diffractometer under the Mo-Kα radiation (λ = 0.71073 Å) generated by a sealed X-ray tube. The diffraction data for [Pt(TD2$^{\bullet}$)(*t*-$BuNH_2$)] were obtained on a Bruker D8 Venture instrument equipped with Mo IμS 3.0 microsource and Photon 3 detector. The measurement temperature was 100 K in all cases. The absorption correction was done using a multi-scan method in *SADABS* (Sheldrick, G. M. University of Göttingen, Germany, 1997). The structures were solved in Olex2 [30] by the ShelXT program [31] using Intrinsic Phasing and refined with the ShelXL package [32] using least squares minimization. All non-H atoms were located in the Fourier map and refined anisotropically. Carbon-bound hydrogen atoms were calculated in ideal positions, with isotropic displacement parameters set to 1.2U_{eq} of the host atom (1.5U_{eq} for methyl hydrogen atoms). Their positions were then refined using a riding model. Q-peaks for hydrogen-bonded N-H protons were located in the Fourier map. The corresponding hydrogens were assigned to those positions and refined explicitly. The essential details pertaining to the experiment and to structure refinement are available in Table S1.

Structure refinement of [Pd(TD2$^{\bullet}$)($PhNH_2$)]. Crystals grew as blue plates by slow evaporation of CH_2Cl_2/pentane under N_2. Data collection was optimized for the triclinic system, and the structures were solved and refined in the triclinic space group P-1. The asymmetric unit cell contained one metal complex. The highest residual Fourier peak found in the model was +0.59 *e* Å^{-3} approx. 0.88 Å from Pd1 and the deepest Fourier hole was -0.43 *e* Å^{-3} approx. 0.74 Å from Pd1.

Structure refinement of [Pt(TD2$^{\bullet}$)(t-$BuNH_2$)]. Crystals grew as blue blocks by slow evaporation of CH_2Cl_2/pentane. collection was optimized for the monoclinic system, and the structures were solved and refined in the monoclinic space group

C2/c. The asymmetric unit cell contained one metal complex. The highest residual Fourier peak found in the model was +1.49 *e* $Å^{-3}$ approx. 0.86 Å from Pt1 and the deepest Fourier hole was -2.87 *e* $Å^{-3}$ approx. 0.87 Å from Pt1.

Structure refinement of [Pt_2(TD2•)$_2$(en)]. Crystals grew as blue plates by slow evaporation of CH_2Cl_2/pentane under N_2. Data collection was optimized for the triclinic system, and the structures were solved and refined in the triclinic space group P-1. The asymmetric unit cell contained one metal complex. The conformation of chlorines Cl1 and Cl2 in one dichloromethane solvent molecule was found to be disordered. The disorder was modeled by splitting the positions of both chlorine atoms over two positions to ensure a stable refinement. The highest residual Fourier peak found in the model was +2.09 *e* $Å^{-3}$ approx. 1.31 Å from H44B and the deepest Fourier hole was -1.80 *e* $Å^{-3}$ approx. 0.66 Å from Cl4.

Electrochemical Measurements

Cyclic voltammograms were performed on a Gamry Reference 600 potentiostat utilizing a single-compartment cell with three electrodes: a glassy carbon working electrode, a platinum wire auxiliary electrode, and a $Ag/AgNO_3$ reference electrode. Measurements were performed at ambient temperature under an inert argon atmosphere in CH_2Cl_2 containing 0.1 M [(*n*-Bu_4)(PF_6)] (triply recrystallized) as a supporting electrolyte. Sample concentrations were 1–2 mM, and all electrochemical data were internally referenced to the ferrocene/ferrocenium couple (set at 0.00 V).

CONCLUSIONS

Three square-planar complexes featuring the tripyrrindione radical $TD2^{2-\bullet}$ and different primary amines, i.e., [Pd(TD2•)($PhNH_2$)], [Pt(TD2•)(*t*-$BuNH_2$)], and [Pt_2(TD2•)$_2$(en)], were synthesized and characterized. The optical absorption and EPR spectra of all complexes confirmed the presence of an unpaired spin delocalized on the tripyrrindione frameworks. In all cases, hydrogen-bonding interactions between the carbonyl groups of the tripyrrindione and the amine ligands led to stable complexes that did not undergo displacement of the amine ligands in the presence of water or other coordinating species in solution at room temperature. Ethylenediamine served as a linker to connect two Pt(II) tripyrrindione radicals in [Pt_2(TD2•)$_2$(en)]. The variable-temperature EPR experiments on toluene solutions of all three complexes indicated the formation at low temperatures of π-dimers through pancake-bonding interactions between tripyrrindione radicals. Electrochemical analysis revealed quasi-reversible tripyrrindione-based oxidation and reduction events in all cases, and the recorded half-wave potentials were cathodically shifted relative to those previously reported for similar tripyrrindione complexes featuring the aqua ligand at the fourth coordination position. Both spectroscopic and electrochemical data indicate that the two Pt(II)-tripyrrindione units in [Pt_2(TD2•)$_2$(en)] behave as independent complexes when connected by the flexible ethylenediamine linker. Overall, this study details the first examples of tripyrrindione complexes featuring aromatic and aliphatic amines, as well as the opportunity offered by these versatile ligands to connect tripyrrindione radicals.

Acknowledgements

This work was supported by the National Science Foundation (award CHE-2203361 to E.T.). The Bruker NEO-500 spectrometer and the Bruker D8 Venture diffractometer in the UArizona Dept. of Chemistry and Biochemistry NMR Facility and X-ray Diffraction Facility, respectively, were purchased thanks to support from the National Science Foundation (MRI awards CHE-1920234 and CHE-2117516).

REFERENCES

1. Falk, H. *The Chemistry of Linear Oligopyrroles and Bile Pigments,* vol. 1. Springer Vienna: Vienna, 1989.
2. Rockwell NC, Lagarias JC. *ChemPhysChem* 2010; **11**: 1172–1180.
3. Wood TE, Thompson A. *Chem. Rev*. 2007; **107**: 1831–1861.
4. Bröring M. In *Handbook of Porphyrin Science,* Vol.8, World Scientific Publishing Company, 2010; pp 343–501.
5. Li C, Kräutler B. *Dalton Trans*. 2015; **44**: 10116–10127.
6. Tomat E. *J. Porphyrins Phthalocyanines* 2019; **23**: 1265–1272.
7. Ding Y, Tang Y, Zhu W and Xie Y. *Chem. Soc. Rev*. 2015; **44**: 1101–1112.
8. Balch AL and Bowles FL. In *Handbook of Porphyrin Science*, Vol. 8, Kadish KM, Smith KM and Guilard R. (Eds.) World Scientific: Singapore, 2010; pp. 293–342.
9. Tomat E, Curtis CJ. *Acc. Chem. Res*. 2021; **54**: 4584–4594.
10. Yamaguchi T, Shioji I, Sugimoto A, Komoda Y and Nakajima H. *J. Biochem*. 1994; **116**: 298–303
11. Hamchand R, Hanley D, Prum RO, Brückner C. *Sci Rep* 2020; **10**: 11264–11274.
12. Gautam R, Loughrey JJ, Astashkin AV, Shearer J, Tomat E. *Angew. Chem. Int. Ed*. 2015; **54**: 14894–14897.
13. Bahnmüller S, Plotzitzka J, Baabe D, Cordes B, Menzel D, Schartz K, Schweyen P, Wicht R, Bröring M. *Eur. J. Inorg. Chem*. 2016: 4761–4768.
14. Gautam R, Astashkin AV, Chang TM, Shearer J, Tomat E. *Inorg. Chem*. 2017; **56**: 6755–6762.
15. Tomat E, Curtis CJ, Astashkin AV, Conradie J, and Ghosh A. *Dalton Trans*. 2023; **52**: 6559–6568.
16. Gautam R, Petritis SJ, Astashkin AV, Tomat E. *Inorg. Chem*. 2018; **57**: 15240–15246.
17. Roth SD, Shkindel T and Lightner DA. *Tetrahedron* 2007; **63**: 11030–11039.
18. Swain A, Cho B, Gautam R, Curtis CJ, Tomat E and Huxter V. *J. Phys. Chem. B* 2019; **123**: 5524–5535.
19. Umetani M, Tanaka T, Osuka A. *Chem. Sci*. 2018; **9**: 6853–6859.
20. Nishiyama A, Tanaka T. *J. Porphyrins Phthalocyanines* 2022; **26**: 815–820.
21. Curtis CJ, Astashkin AV, Conradie J, Ghosh A, Tomat E. *Inorg. Chem*. 2021; **60**: 12457–12466.
22. Curtis CJ, Tomat E. *J. Porphyrins Phthalocyanines* 2020; **24***:* 112–120.
23. Wilson JJ, Lippard SJ. *Chem. Rev*. 2014; **114**: 4470–4495.
24. Preuss KE. *Polyhedron* 2014; **79**: 1–15.
25. Kertesz M. *Chem. – Eur. J*. 2019; **25**: 400–416.
26. Bröring M, Brandt CD, Link S. *Inorg. Chim. Acta* 2005; **358**: 3122–3134.
27. Maity M, Das S, and Maiti NC. *Phys. Chem. Chem. Phys*. 2005; **16***:* 20013–20022.
28. Yang B, Taylor RC, Morris MD, Wang XZ, Wu J, Yu BZ, Xu G, and Soloway RD. *Spectrochimica Acta Part A: Molecular Spectroscopy* 1993; **49**:1735–1749.
29. Zanello P, Connelly NG. *Inorganic Electrochemistry: Theory, Practice and Application*. Royal Society of Chemistry: Cambridge, 2003
30. Dolomanov OV, Bourhis LJ, Gildea RJ, Howard JAK, Puschmann H. *J. Appl. Crystallogr*. 2009; **42**: 339–341.
31. Sheldrick GM. *Acta. Crystallogr. Sect. A* 2015; **71**: 3–8.
32. Sheldrick GM. *Acta. Crystallogr. Sect C* 2015; **71**: 3–8.

Primary amines as ligands and linkers in complexes of tripyrrindione radicals

Iva Habenšus, Ameen Ghavam, Clayton J. Curtis, Andrei V. Astashkin, Elisa Tomat*

The tripyrrin-1,14-dione pigments coordinates Pd(II) and Pt(II) to form paramagnetic complexes carrying an unpaired spin within the ligand π system. Primary amines at the fourth coordination site engage in intra-ligand hydrogen bonds with the terminal carbonyl groups of the tripyrrole. Ethylene-1,2-diamine is employed to connect two Pt(II) tripyrrindione complexes and form a stable diradical system.